Bayesian optimisation for CPT-based prediction of impact pile driveability

Róisín Buckley[1], Yuling Max Chen[2], Brian Sheil[3], Stephen Suryasentana[4], Diarmid Xu[5], James Doherty[6],

Mark Randolph[7]

[1]Lecturer, James Watt School of Engineering, University of Glasgow, UK. Email: roisin.buckley@glasgow.ac.uk.

[2]PhD candidate, Department of Statistics and Actuarial Science, University of Waterloo, Canada formerly Department of Engineering Science, University of Oxford. Email: yuling.chen@uwaterloo.ca

[3]Laing O'Rourke Associate Professor in Construction Engineering, Department of Engineering, University of Cambridge, UK. Email: <bbs24@cam.ac.uk>

[4]Chancellor's Fellow (Lecturer), Department of Civil & Environmental Engineering, University of Strathclyde, U.K. Email: stephen.suryasentana@strath.ac.uk.

[5]PhD candidate, Department of Engineering, University of Cambridge, Cambridge, UK. Email: dmx20@cam.ac.uk.

[6]Associate Professor, Department of Civil, Environmental and Mining Engineering, University of Western Australia, Australia. Email: james.doherty@uwa.ed.au

[7]Emeritus Professor, Department of Civil, Environmental and Mining Engineering, University of Western Australia, Australia. Email: mark.randolph@uwa.ed.au

Word count: 5775

Tables: 4

Figures: 18

ABSTRACT

Pile driveability predictions require information on the pile geometry, impact hammer and the soil resistance to driving (SRD). Current SRD prediction methods are based on databases of long slender piles from the oil and gas industry and new, robust and adaptable methods are required to predict SRD for current offshore pile geometries. This paper describes an optimisation framework to update uncertain model parameters in existing axial static design methods to calibrate SRD. The approach is demonstrated using a case study from a German offshore wind site. The optimisation process is undertaken using a robust Bayesian approach to dynamically update uncertain variables during driving to improve simulations The existing method is shown to perform well for piles with geometries that reflect the underlying database such that only minimal optimisation is required. For larger diameter piles, relative to the prior best estimate, optimised results are shown to provide significant improvements in the mean calculations, and associated variance, of pile driveability as more data is acquired. When compared with results determined using the conventional design approach used by industry, the optimised parameters provided notable improvements in the agreement between measured and calculated values. The optimised parameters can be used to predict SRD in similar profiles and the demonstrated framework may be used to develop new SRD methods where large datasets are available.

.

INTRODUCTION

Offshore wind turbines (OWT) are typically supported by driven open-ended steel piles as either one of multiple axially loaded foundations for a jacket structure or single, large-diameter laterally loaded monopiles. Typical jacket piles range in diameter from 2.5-3m with length-to-diameter ratios (*L/D*) between 7 and 20 (P. Barbosa, personal communication, 2021). The size of monopile foundations is increasing rapidly; in current and future projects diameters range from 6-11m with *L/D* ratios of 3-5 (Siegl et al., 2020). Both foundation types are installed in the offshore environment using large hydraulic impact hammers. When a hammer strikes a pile, a stress wave is generated which travels down the pile to the tip. Prior to the installation works pile driveability analyses are used to (i) choose the optimal hammer to size and effectively safely install the pile and (ii) ensure that driving does not induce excessive fatigue stresses in the pile.

Driveability analyses typically use one-dimensional stress wave theory to model the forces and displacements in the pile during driving. The analysis requires information about the pile geometry, the pile penetration, the hammer characteristics and an empirical (or physics-based) method to predict the soil resistance to driving (SRD) or short-term axial capacity provided by the soil. The SRD for a fully coring open-ended pile is given by:

$$SRD = \pi \left(D \int_0^L \tau_f \, dz \right) + A_{ann} q_{ba} \tag{1}$$

where τ_f is the total internal and external driving shaft resistance, L is the pile embedment, A_{ann} is the annular steel area and q_{ba} is the end-bearing resistance acting on the steel annulus. An effective SRD formulation is capable of capturing the primary physical mechanisms of axial pile behaviour during installation, i.e.: (i) links between penetration resistance and in situ tests such as the cone penetration test (CPT) and (ii) reductions in local effective stresses at any given soil horizon with increasing pile penetration, a phenomenon commonly referred to as 'friction fatigue' (Heerema, 1978). Current empirical SRD approaches were developed through back analysis of pile driving records in sands, clays and rocks (e.g. Toolan and Fox, 1977, Stevens et al., 1982, Alm and Hamre, 2001) using databases of the predominantly slender piles used by the oil and gas industry. Empirical methods that account for 'friction fatigue' or length effects and use in situ tests such as the CPT are convenient for capturing ground variability, both with depth and across large offshore sites, and can offer improved predictability. The most widely adopted SRD method in practice is that developed by Alm and Hamre (2001). Internal and external shaft resistance are not considered separately and in sands, τ_f is calculated

3

as a function of the total corrected CPT cone resistance, q_t, the relative distance of a given soil horizon above the pile tip, h, and the effective overburden pressure, σ'_{vo}:

$$\tau_f = 0.00264\, q_t \left(\frac{\sigma'_{vo}}{p_a}\right)^{0.13} \sigma'_{vo} tan\delta' + \left(0.01056\, q_t \left(\frac{\sigma'_{vo}}{p_a}\right)^{0.13} \sigma'_{vo} tan\delta'\right) e^{-\frac{\sqrt{\frac{q_t}{\sigma'_{vo}}}h}{80}} \tag{2}$$

where δ is the sand-pile interface friction angle. At the base in sands, $q_{ba} = 0.15 q_t (q_t/\sigma'_{vo})^{0.2}$ (3). The method is based on a database of 186 slender piles with diameters of 0.76-2.74m with a mean of 2.24m and a standard deviation of 0.39m and slenderness ratios of 14.4-40.8 with a mean of 25.3 and a standard deviation of 7.1. One pile in the database has an L/D ratio of 151. The formulation of the Alm and Hamre approach makes extrapolation to the emerging OWT pile geometries uncertain; equation (2) does not include a diameter term within the degradation function, likely due to the relatively uniform database employed. Recent studies have highlighted the need for new approaches to predict pile driveability for larger diameter piles. Perikleous et al. (2020) assessed the performance of several empirical methods, including the Alm and Hamre (2001) approach, against installation records of 260 North Sea monopile foundations and found poor prediction accuracy. Maynard et al. (2018) back analysed 202 monopile driving records for piles installed in a range of ground conditions and found variable results, with significant over-prediction using the Alm and Hamre (2001) method for the sands and clays at two out of three sites. They proposed empirical fitting parameters to resolve the differences between their observations and the results obtained with the Alm and Hamre (2001) method.

CPT-based static axial design methods, intended to predict medium-term pile capacity, have gained popularity in recent years and have been used in SRD predictions with variable success (see e.g. Byrne et al., 2012, Byrne et al., 2018, Schneider and Harmon, 2010). Lehane et al. (2020) describe a new 'unified' method to predict static axial pile capacity in sands which draws together the four CPT-based methods recommended in API (2014). For full-scale (D>1m) circular offshore pipe piles in compression, at a time of two weeks after installation, the shaft friction is calculated from:

$$\tau_f = 0.0125 q_c \left[max\left(\frac{h}{D}, 1\right)\right]^{-0.4} \left[1 - \left(\frac{D_i}{D}\right)^2\right]^{0.3} \tag{4}$$

Where q_c is the uncorrected cone resistance and D_i is the internal pile diameter. The base pressure applied over the pile's gross base area, q_{bg}, is taken as $0.15 q_{c,avg}$ where $q_{c,avg}$ is the cone resistance within a zone extending 1.5D above and below the tip. The unified database consisted of static load tests on 71 piles (31 closed-ended

and 40 open-ended) in siliceous sand. The open-ended piles in the database have diameters of 0.34-2m with an average of 0.66m and a standard deviation of 0.32m and an average L/D ratio of 28.9 with a standard deviation of 14.22. Two piles at Mobile Bay (not shown on Figure 1) had diameters of 0.32m and penetrations of 42.4m giving L/D ratios of 132.5.

Figure 1 illustrates the spread of L/D ratios and penetrations for the Alm and Hamre (2001) and Lehane et al. (2020) unified sand databases as well as typical monopile and jacket pile geometries used to support OWTs. Current OWT jacket piles have L/D ratios that lie at the lower end of the Alm and Hamre (2001) calibration space and are well outside the static database ranges. Monopile foundations can be seen to fall outside of the parameter space of both the SRD and axial methods.

The static formulation has the benefit that (i) it follows established physical mechanisms that are supported by observations obtained in instrumented pile tests (Lehane et al., 2020) and (ii) it accounts for pile scale in the formulations, through inclusion of a diameter term, allowing extrapolation to different geometries. While the axial static design method appears more flexible, there are three main obstacles to using the method in its current form to calculate SRD: (i) the long-term static pile capacity was calibrated for fully equalised or aged piles and is therefore likely higher than the SRD, (ii) both the ultimate pile tip movement and the behaviour of the internal soil plug during a static test is expected to be different to that induced during driving, and (iii) the underlying databases, while carefully collated and curated, are limited to particular ground conditions and pile geometries (there are no available data for piles with D>2m). It is also worth noting that the recently developed ICP Chalk-18 formulation for SRD (Buckley, 2018, Jardine et al., 2023), calibrated against large diameter piles, required inclusion of an additional dependence of both the exponent on the degradation term (equivalent to -0.4 in Eq (4)) and the mobilisation of base resistance on the on D/t ratio to capture the response across a range of pile geometries.

Given the large-scale nature of next-generation offshore wind farms (OWF), considerable savings can be realised if a more optimal, automated and adaptive approach to pile installation prediction at OWF sites is adopted. This paper describes an optimisation framework which is used to update uncertain model parameters in the axial static design method for the prediction of pile driveability. The optimisation process is undertaken using a robust Bayesian approach to dynamically update uncertain variables during driving to improve predictions. Pile driveability predictions in this study were preformed using industry-standard 1D wave

5

equation analyses. Tsetas et al. (2021) compared 1D models with a 3D model that accounted for wave dispersion and non-local soil reaction and showed that the 1D models become less accurate for diameters greater than ≈4m, above the maximum D considered in this study. The approach is demonstrated using a previously published case study from a German offshore wind site. The ground conditions and pile installation at the Wikinger OWF were described in detail by Barbosa et al. (2015), Buckley (2018), Buckley et al. (2020) and Buckley et al. (2021).

SITE LOCATION AND PILE DETAILS

The case study focuses on driving of the 1.37m diameter (L/D=8.6, diameter-to-wall thickness (D/t) ratio=34) steel pipe 'pre-construction' test piles (TP) and 2.7m diameter 'production piles' (PP) (L/D=5.9 D/t=53) at two wind turbine generator (WTG) locations (Figure 2) through Holocene and Pleistocene glacial till layers, which overlie the low-medium density Maastrichtian chalk at the site. The till classifies as silty sand and sandy silt with q_t typically between 3 and 30 MPa and f_s, typically between 100 and 300 kPa but in some cases as high as 1MPa (see Figure 3). Excess penetration pore pressures, measured at the u_2 position, showed generally negative values of -100 to -250 kPa ~~with discrete peaks up to +1 MPa~~. Loose Holocene sand deposits were found in the upper 1.9m. Particle size distributions for the materials considered in this study are shown on Figure 4. Buckley et al. (2020) identified the low-plasticity glacial till as silty/clayey sand with ≈10% clay content; consequently the glacial till is treated as a sand for the purposes of the pile driveability calculations reported in this study.

The "pre-construction" trial campaign involved driving of three identical 1.37m diameter test piles (TPs; WK38-1, WK38-2 and WK38-3), spaced ~8m apart. Two of the piles (WK38-1 and WK38-2) were instrumented with accelerometers and strain gauges near the pile head and monitored dynamically during driving whereas the third pile (WK38-3) recorded only blow counts and pile energies during installation. Buckley et al. (2020) detail the back analysis of the driving signals with IMPACT for mid-driving and end of driving blows at WK38-1 and WK38-2. Four 2.7m diameter 'production' piles (PP-E, PP-S, PP-W and PP-N) were eventually installed at each WTG location to support the jacket structures.

Self-weight penetrations of on average 1.9m with a standard deviation of 0.8m were recorded before the start of driving. The TPs were installed with a Menck MHU 800-S hydraulic hammer while the PPs were installed with an MHU 1200-S hydraulic hammer. Due to the limited number of datapoints recorded during driving of

6

the WK38 production piles, a production pile at another WTG location in similar ground conditions was also considered. The recorded hammer blow counts and measured hammer energies for the piles considered in this study are plotted in Figure 5. For the TP piles, the energy per blow applied reached a stable value of 500kJ once the piles had been driven approximately 2m and the blow counts increased accordingly with depth. The energy per blow was increased steadily during driving of the PP piles, resulting in a relatively constant trend in blow count with depth.

MODELLING OF PILE DRIVEABILITY

Dynamic analysis

The driveability calculations in this study were performed using the one-dimensional wave equation code IMPACT (Randolph, 1990, Randolph, 2008) which employs the method of characteristics (De Josselin de Jong, 1956) as a numerical method. A web-based version of the program is available at geocalcs.com. Several soil rheological models of varying complexity have been developed to model the response during driving (see e.g. Simons and Randolph, 1985, Deeks and Randolph, 1993, Salgado et al., 2015, Kaynia et al., 2022). While IMPACT includes several of these advanced options to model the soil and base resistance, the pile driving soil base and shaft resistances in this study were modelled in this study using the Smith (1962) approach. While the limitations of the Smith approach are well documented (see e.g. Buckley et al., 2017) it remains the most commonly employed tool by industry for simple and practical driveability analysis. The shaft resistance is modelled at each node along the pile length using linear springs and a plastic slider (see Figure 6), representing the relative movement between the pile and the soil and the static shaft resistance respectively. A dashpot is also included which accounts for all soil damping effects. While explicit modelling of the internal soil plug is possible in IMPACT, here the internal friction has been set to zero for simplicity, i.e. with no interaction between pile and soil plug. The shear stress at any node along the discretised pile length is given by:

$$\tau = \min\left(\frac{w}{U_{q,s}}, 1\right)(1 + J_s v)\tau_f \tag{5}$$

where $U_{q,s}$ is the shaft soil displacement or "quake" required to mobilise the static shaft resistance τ_f, w is the vertical nodal displacement, J_s is a shaft damping parameter and v is the pile nodal velocity. The base resistance is modelled in a similar manner:

7

$$q_b = \min\left(\frac{\text{w}}{\text{U}_{\text{q,b}}}, 1\right)(1 + \text{J}_b\text{v})q_{ba} \qquad (6)$$

While the quake and damping parameters can have a significant influence on driving behaviour, values of these parameters from the literature lie within a relatively narrow range. Fixed values have been adopted for the Smith parameters in this study (i) for simplicity and to demonstrate the optimisation framework and (ii) to compare with predictions made with the conventional SRD approach. However it is accepted that these parameters may also vary with soil type and pile geometry and be affected by the limitations of the method.

The quake at the shaft and toe was taken as 2.5mm while the shaft damping and base damping parameters were adopted as 0.25s/m and 0.5s/m respectively consistent with Alm and Hamre (2001). Various approaches can be used to model the impact between the hammer and the pile. While precise modelling of the impact can be complex, for the purposes of driveability studies, the main features can be simulated by relatively simple models shown to replicate field measurements; Randolph (2008). In this study, the hammer impact was modelled using the analytical solution of Deeks and Randolph (1993) implemented in IMPACT. The model requires the mass of the hammer ram (m_r) and anvil (m_a) as input, a cushion stiffness (K_c), as well as the applied energy or impact velocity taken from the driving records. The adopted hammer parameters are shown in Table 1. No energy losses have been assumed and a high cushion stiffness ($2.8\text{x}10^7$kN/m) was adopted to ensure the modelled hammer force-time signature response reflected that observed on the instrumented piles.

Deterministic SRD model

While IMPACT uses the Smith (1962) approach to model the soil resistance, an estimate of the shear stress, τ_f, along the pile length and the end-bearing must be first determined using an empirical SRD model. This paper focuses on deterministic SRD models such that the model predictions are obtained as an explicit function of the model inputs and the measured CPT data. To demonstrate the applicability of the optimisation framework, the form of the static axial design method described previously is adopted to calculate soil penetration resistances acting along the pile shaft and at the pile base.

$$\tau = a_{s1}q'_{\text{t}}\left[\max\left(\frac{h}{D}, a_{s2}\right)\right]^{-a_{s3}}\left[1 - \left(\frac{D_{\text{i}}}{D}\right)^2\right]^{a_{s4}} \qquad (7)$$

where a_{s1}, a_{s2}, a_{s3} and a_{s4} are model parameters. The generic formulation also adopts q'_t in place of the uncorrected cone resistance, q_c used in the original formulation (and q_t in the Alm and Hamre calculations;see Eq(2)) where q'_t is the total cone resistance less the hydrostatic pore water pressure, u_0. Consistent with the static formulation for sands, the base pressure is taken as equal to $b_s q'_{t,avg}$ (Eq 8) where $q'_{t,avg}$ is the cone end resistance averaged $1.5D$ above and below the pile toe, and applied over the full gross base area of the pile. In the original formulation the latter is intended to replicate the capacity during slow static loading, where the pile behaves as fully plugged. Large diameter open-ended piles tend to drive in a 'fully coring' (or unplugged) manner and the potential use of Eq 7 to calculate base capacity mobilised during a hammer blow, which encompasses both the base resistance on the annular tip and any contribution of internal friction form the soil plug, is uncertain and requires further investigation.

Uncertain parameters

For equations (7) and (8) the greatest uncertainty relates to the soil penetration resistances; the SRD model input parameters are therefore treated as uncertain variables to be updated sequentially during driving as shown in Figure 7. The vector of uncertain variables, $\boldsymbol{\theta}$, can be defined as:

$$\boldsymbol{\theta} = [\, a_{s1}, a_{s2}, a_{s3}, a_{s4}, b_s]\tag{9}$$

The recommended empirical values given previously (see Eq (4)) are taken as the best prior estimate of $\boldsymbol{\theta}$. A default coefficient of variation (COV) of 0.3 has been adopted for all parameters in $\boldsymbol{\theta}$ to achieve 'weak' priors such that the posterior distributions are largely dictated by the likelihood distributions (monitored data). Future access to larger databases of monitored data will allow researchers to 'tune' the COV values to the relative confidence in specific parameters.

BAYESIAN OPTIMISATION

Overview

Calibration of empirical models with observed performance, either in the field or in physical model tests, is common in geotechnical applications (e.g. Jardine et al., 2005, API, 2014). Bayesian updating is a popular method due to its ability to handle noisy and missing data and for its explicit treatment of uncertainty in the

updating process e.g. Hsiao et al. (2008), Zhang et al. (2009), Hsein Juang et al. (2013), Collico et al. (2022). The model adopted in this paper is defined as follows:

$$\boldsymbol{y} = g(\boldsymbol{\theta}) + \varepsilon \tag{10}$$

where $\boldsymbol{y} = [y_1, y_{2,\dots}, y_n]$ is the vector of calculated penetrations per blow corresponding to strokes $\boldsymbol{x} = [x_1, x_2,\dots,x_n]$, n is the number of observed data points used for Bayesian updating, $g(\boldsymbol{\theta})$ denotes the IMPACT calculated penetration per blow using the soil resistances defined by equation (7) and (7), and ε is a noise term that captures the model and measurement errors, and is assumed to follow a normal distribution with mean, μ_e = 0 and standard deviation σ_e as adopted in many practical domains (Jaynes and Bretthorst, 2003). It is noteworthy that $g(\boldsymbol{\theta})$ is now a stochastic variable due to the use of uncertain input parameters in the deterministic calculation model. In this paper, the notation $p(A|B,C)$ refers to the probability of event A, given that events B and C have occurred - also referred to as conditional probability.

The information to be updated is the joint probability distribution of the random variable $\boldsymbol{\theta}$. To prevent negative realisations of the non-negative model input parameters $\boldsymbol{\theta}$, a lognormal distribution is adopted for the uncertain variables (Lumb, 1966, Qi and Zhou, 2017, Li et al., 2016, Zheng et al., 2018). Therefore, the natural logarithm of $\boldsymbol{\theta}$ follows a multivariate normal distribution with mean $\boldsymbol{\mu'_\theta}$ and standard deviation $\boldsymbol{\sigma'_\theta}$, i.e., $\boldsymbol{\theta'} \equiv \ln(\boldsymbol{\theta}) \sim MVN(\boldsymbol{\mu'_\theta}, \boldsymbol{\sigma'_\theta})$. As each model parameter plays a different role and has a different practical meaning, the parameters are assumed to be independent. Whilst the consideration of parameter inter-dependence can be achieved using multivariate statistical distributions, this would incur a significant increase in computational costs and complexity. Therefore, the joint prior probability distribution of the random variable $\boldsymbol{\theta'}$ is a product of the prior distributions of the parameters:

$$p(\boldsymbol{\theta'}|\boldsymbol{\mu'_\theta}, \boldsymbol{\sigma'_\theta}^2) = \prod_{i=1}^{9} \frac{1}{\sqrt{2\pi\sigma_{\theta_i}'^2}} e^{-\frac{1}{2}\left(\frac{\theta_i' - \mu_{\theta_i}'}{\sigma_{\theta_i}'}\right)^2} \tag{11}$$

where θ_i' is the i-th entry of the vector parameter $\boldsymbol{\theta'}$, e.g., $\theta_1' = a_{s1}$.

The mean $\boldsymbol{\mu_\theta}$ and variance $\boldsymbol{\sigma_\theta^2}$ for the prior variable $\boldsymbol{\theta}$ are calculated as:

$$\mu = \ln\left(\frac{\mu_\theta^2}{\sqrt{\mu_\theta^2 + \sigma_\theta^2}}\right) \qquad \sigma^2 = \ln\left(1 + \frac{\sigma_\theta^2}{\mu_\theta^2}\right)$$

Updating model predictions using driving data

The prior lognormal distributions of the model input parameters are updated to account for the data y, using the likelihood function $p(y|\theta,x)$, to produce 'posterior' distributions of θ. The likelihood function describes the probability of predicting the observed driving data using the existing model for particular values of the parameter vector θ:

$$p(y|\theta, x) = \prod_i p(y_i|\theta, x) \tag{12}$$

The posterior distribution of the model parameters, $p(\theta|x, y)$, is obtained using Bayes' theorem as follows:

$$p(\theta|x, y) = \frac{p(y|\theta, x)\, p(\theta|x)}{p(y|x)} \tag{13}$$

$p(y|x)$ in equation (12) normalises the joint posterior distribution to ensure that it integrates to one and is obtained by marginalising out θ, as follows:

$$p(y|x) = \int p(y|\theta, x)p(\theta|x)d\theta \tag{14}$$

Monte Carlo Sampling

Markov Chain Monte Carlo (MCMC) is one of the most popular techniques for Bayesian inference problems to generate samples from posterior probability distributions for which Bayes' theorem does not yield closed-form solutions, such as equation (14). However, common MCMC samplers, such as Hamiltonian Monte Carlo samplers, are gradient-based methods and gradient information for complex models is often intractable. Sequential Monte Carlo (SMC) samplers differ from common MCMC methods in that the SMC sampler gradually samples the "intermediate" probability density functions (PDFs) from the prior to the posterior distribution, and a population of iteratively reweighted samples evolves over several loops of simple MCMC sampling procedure (e.g., Metropolis Hasting MC).

The SMC method recasts the posterior distribution given by equation (14) as follows:

11

$$p(\boldsymbol{\theta}|\boldsymbol{x},\boldsymbol{y})_{\text{SMC}} \propto p(\boldsymbol{y}|\boldsymbol{\theta},\boldsymbol{x})^{\beta} p(\boldsymbol{\theta}|\boldsymbol{x}) \tag{15}$$

where β is the 'tempering' parameter such that $\beta = 0$ recovers the *prior* and $\beta = 1$ recovers the *true posterior*. The parameter β therefore allows tuning of the sampling by incrementally introducing the importance of the likelihood function. The SMC sampler used in the current study is based on the 'Cascading Adaptive Transitional Metropolis In Parallel' (CATMIP) algorithm (Minson et al., 2013) which itself is based on the Transitional Markov Chain Monte-Carlo (TMCMC) algorithm (Ching and Cheng, 2007).

The parameter sampling process is designed as follows, following Ching and Chen (2007).

1. Initialize the tempering parameter $\beta_0 = 0$ and generate N samples from the prior to create set $S_{\beta_0} = \left\{\boldsymbol{\theta}_k^{(0)}\right\}_{k=1,\dots,N}$. Intialize $i = 0$.

2. Choose $\beta_{i+1} > \beta_i$ such that the coefficient of variation (COV) of the "plausibility weights"

$$w\left(\boldsymbol{\theta}_k^{(i)}\right) = p\left(\boldsymbol{y}|\boldsymbol{\theta}_k^{(i)},\boldsymbol{x}\right)^{\beta_{i+1}-\beta_i}, k = 1,\dots,N$$

   is maintained at a prespecified threshold ξ (default set to 0.5 in our analysis).

3. Initialize N Markov chains each starting with the elements in the sample set S_{β_i}, i.e., $\boldsymbol{\theta}_k^c = \boldsymbol{\theta}_k^{(i)}, k = 1,\dots,N$. (The subscript "c" denotes "current".)

4. With probability $\frac{w\left(\boldsymbol{\theta}_k^{(i)}\right)}{\sum_{l=1}^{N} w\left(\boldsymbol{\theta}_l^{(i)}\right)}$, conduct a Metropolis-Hasting MC along the k-th Markov chain to sample $\boldsymbol{\theta}_k^{(i+1)}$ with a Gaussian proposal PDF, i.e., sample $\boldsymbol{\theta}'$ from $N(\boldsymbol{\theta}_k^c, \Sigma_j)$ with

$$\Sigma_j = \gamma^2 \cdot \sum_{k=1}^{N} w\left(\boldsymbol{\theta}_k^{(i)}\right) \left[\boldsymbol{\theta}_k^{(i)} - \frac{\sum_{l=1}^{N} w\left(\boldsymbol{\theta}_l^{(i)}\right)\boldsymbol{\theta}_l^{(i)}}{\sum_{l=1}^{N} w\left(\boldsymbol{\theta}_l^{(i)}\right)}\right] \cdot \left[\boldsymbol{\theta}_k^{(i)} - \frac{\sum_{l=1}^{N} w\left(\boldsymbol{\theta}_l^{(i)}\right)\boldsymbol{\theta}_l^{(i)}}{\sum_{l=1}^{N} w\left(\boldsymbol{\theta}_l^{(i)}\right)}\right]^T$$

   where γ is a scaling factor prespecified as 0.2 by default.

   With probability $min\left\{1,\frac{p(\boldsymbol{\theta}')}{p(\boldsymbol{\theta}_k^c)}\right\}$, accept the new proposal $\boldsymbol{\theta}_k^{(i+1)} = \boldsymbol{\theta}'$ and update the current parameter $\boldsymbol{\theta}_k^c = \boldsymbol{\theta}'$; otherwise reject the proposal and retain the current parameter $\boldsymbol{\theta}_k^{(i+1)} = \boldsymbol{\theta}_k^c$.

5. Repeating step 4 N times outputs a collection of N samples from $p(\boldsymbol{y}|\boldsymbol{\theta},\boldsymbol{x})^{\beta_{i+1}} p(\boldsymbol{\theta}|\boldsymbol{x})$, denoted as $S_{\beta_{i+1}} = \left\{\boldsymbol{\theta}_k^{(i+1)}\right\}_{k=1,\dots,N}$.

6. $i \leftarrow i + 1$ and repeat step 2-5 until $\beta_{i+1} = 1$.

7. The final result is a collection of N samples from the posterior

$$p(\boldsymbol{\theta}|\boldsymbol{x}, \boldsymbol{y})_{\text{SMC}} \propto p(\boldsymbol{y}|\boldsymbol{\theta}, \boldsymbol{x})p(\boldsymbol{\theta}|\boldsymbol{x}).$$

The increment of the tempering parameter β reflects the difficulty of identifying the posterior distribution; the more difficult the distribution is to identify, the smaller the increment of β, and thereby the more steps it takes for the reweighted samples to evolve from prior to posterior. This framework was developed using PyMC3 programming in Python 3.6.

Methodology

The first optimisation involved updating the default prior parameters from Lehane et al. (2020) using measured installation data from TP WK38-3 (D = 1.372 m), the only pile installed without dynamic monitoring. This pile represents a typical dataset of an unmonitored OWT foundation pile. The performance of the optimised parameter set from this 'prototype' pile was assessed by performing unseen predictions on identical piles WK38-1 and WK38-2, which benefit from close proximity to the optimisation pile. The second optimisation involved updating the same default prior parameters, this time using measured installation data from the larger diameter PP (D = 2.7m). Unseen calibrations are subsequently performed on three additional identical PPs at the same location. The adopted framework is illustrated on Figure 8.

RESULTS & DISCUSSION

Calibration pile WK38-3

Figure 9 shows the pile driveability calculations, in terms of pile penetration per blow, using the prior Lehane et al. (2020) parameters as well as the SMC optimised SRD parameters updated at 25%, 50%, 75% and 100% of the final penetration. Note that the results terminate at ~11.7m to coincide with the maximum CPT depth. For the SMC analyses, in addition to the mean result, 500 realisations of the model obtained by sampling values of the posterior distribution of $\boldsymbol{\theta}$ are shown using light grey lines.

Figure 9 (a) shows that for the 1.37m diameter test pile considered here, the prior Lehane et al. (2020) parameters provide reasonable estimations of the displacement per blow, illustrating the suitability of the static formulations for pile driveability predictions. This is not surprising given that the Lehane et al. (2020) priors were derived from heuristic back-analysis of tests on piles with similar geometries, albeit for static analysis. The reasonably good match between driving resistance and static capacity (intended to reflect the value at 14

13

days after driving) suggests that changes in capacity in this period were small and provides confidence in the suitability of the static formulations to predict SRD. As more data is acquired, the agreement between the SMC calculations and measured data generally improves and an even closer agreement overall between measured and predicted displacements can be observed at the end of driving (see Figure 9 (e)). The final sets of optimised parameters at the end of driving are compared with the default priors in Table 2 (mean values) and Table 3 (COV). In general, the updating process causes reductions in the COV for the model parameters.

The results of the parameter optimisation process are presented in Figure 10 and summarised in Table 2. Shaded regions denote the 90% confidence interval associated with the SMC optimised parameters. Figure 9 and Figure 10 illustrate that the respective optimised values of the model parameters appear to be well approximated by the Lehane et al. (2020) priors with changes typically of ~10% . The 90% CI indicates that the optimisation yields improvements in the certainty of all parameters with COV reducing to between 0.13 and 0.25. The shapes of the updated (posterior) distributions of θ are compared to the prior distribution in Figure 11 for selected update points during the driving of WK38-3. The parameters are shown to experience a negligible shift in the posterior distributions but notable increases in the strength of the distribution are shown for parameters as_2, as_3 and b_s.

The influence of the parameter updating process on the IMPACT-calculated variation of capacity (Figure 12 and Table 4) reflect the trends seen in Figure 9 to Figure 11. There is very little change in shaft capacity (<4%) reflecting the small changes in these parameters. The base capacity reduces by ≈12% consistent with the change in b_s seen in the posterior means. At the final update point, the optimised shaft capacities in the till are lower than those predicted by both the Alm and Hamre (2001) and those back analysed from driving signals at neighbouring piles using more advanced soil resistance models (Buckley et al. (2020)). The optimised base capacities are ≈2.6 and 1.9 times the Alm and Hamre (2001) and signal back analysed values respectively, reflecting the application of q_{bg} to the piles' gross area.

Figure 13(a) presents a summary of IMPACT accuracy using three different SRD models: (i) the "static" sand formulation with prior parameters, (ii) the same formulation with SMC optimised parameters, and (iii) the industry-standard Alm and Hamre (2001) approach for sands. The accuracy has been determined as follows:

$$Accuracy = \frac{p_{\text{calc}} - p_{\text{meas}}}{p_{\text{meas}}} \qquad (16)$$

where p_{pred} and p_{meas} are the calculated and measured (respectively) penetrations per blow for a given pile embedment depth. The Alm and Hamre (2001) approach tends to over-estimate the penetration per blow while the IMPACT calculations using prior parameters provide reasonable estimates which are marginally improved using the SMC optimisation. Both the prior and SMC optimised formulations perform better than the Alm and Hamre (2001) method, illustrating the potential of these methods for use in SRD predictions with further development.

Unseen verification piles WK38-1 and WK38-2

SMC driveability predictions for WK38-1 and WK38-2 using the optimised parameters at the end of driving are compared with those determined using the default prior Lehane et al. (2002) parameters in Figure 13. It is worth noting that the same pile geometry and CPT data are used here; only the energy varies between the identical piles. Driveability predictions using the prior parameters generally provide a slight under-prediction of the measured penetration per blow which is improved using the optimised parameters. While the optimised parameters provide improved agreement with the measured data compared with the prior estimates, some divergence between IMPACT predictions and the field measurements, particularly in the region between 0 and 4m remains, reflecting residual uncertainty in the optimised parameters and likely variations between the ground conditions at the three locations for which only one CPT is available. Additional driving data provided to the optimisation process may have further reduced the variation between these profiles and led to an even stronger agreement between the SMC simulations and the measured data.

Calibration pile PP-E

An additional calibration exercise was carried out using the larger diameter (2.7m) PP at a WTG location (PP-E; see Figure 2 and Figure 3). It is worth noting that the optimised parameters from the 1.37m diameter piles provided a poor fit to the observations at this location, possibly due to inadequate treatment of pile-geometry-scale effects in the existing formulation. During the second optimisation, the same parameters were updated using the field measurements from the installation. Driveability calculations using the SMC optimised SRD parameters are plotted as a function of the pile tip embedment depth in Figure 14 and the results of the SMC parameter optimisation process are presented in Figure 15. In this case, prior predictions using the default

15

parameters provide a poor estimate of the pile driveability, as shown in Figure 14 (a). Subsequent updates of the model parameters (at 25%, 50%, 75% and 100% of final penetration) serve to significantly improve the confidence in the results where very good agreement with the measured field data is obtained at the end of driving (stroke 1125; Figure 14 (e)).

The SMC mean result shows good convergence of the shaft friction parameters a_{s1}, a_{s2} and a_{s3} over the drive (see Figure 15). Parameter $a_{s4,}$ the exponent on the diameter term in Eq 3, showed a reduction from 0.3 to 0.225. The greatest change was in the base parameter b_s (Figure 15 (e)) which showed a significant increase over the drive from 0.15 to 0.29. Similar to the optimisation at WK38-3, the optimised values of parameters $a_{s1,}$ a_{s2} and a_{s3} appear to be well approximated by the Lehane et al. (2020) priors. The final COV for base parameter b_s (see Table 3) indicates important residual uncertainty.

The shape of the updated (posterior) distributions of θ are compared to the prior distribution in Figure 16 for selected update points during the driving of PP-E. The distributions for a_{s1}, a_{s2} and a_{s3} are well approximated by the priors showing negligible shift in the posterior distribution but notable increases in the strength of the distribution (Figures 15 (a) -(c) respectively). There appears to be no obvious convergence for parameter a_{s4} at the final update point. For parameter b_s, the updating process causes significant changes to the posterior distribution where the final posterior distribution has been shifted to the right and has transitioned towards a bimodal shape, possibly due to the underdetermined nature of the optimisation problem and the non-uniqueness of the final solution.

The variation of shaft resistance is shown on Figure 17 and Table 4 for this pile. Similar to the optimisation at WK38-3, the shape of the profiles is comparable between the prior and posterior calculations. The updating exercise leads to an increase in the overall predicted shaft resistance of ≈14% higher reflecting the reduction in degradation parameter a_{s1}. In contrast to the smaller diameter WK38-3, which showed only small changes in base capacity, the optimisation process leads to an almost doubling in base capacity compared to the calculation with the priors, This possibly reflects a larger contribution from internal shaft friction for the L/D=5.9 production piles than the more slender test piles and/or the higher relative tip movement of 3%D (and therefore higher mobilisation of base resistance; see Gavin and Lehane (2007)) compared to the ≈1%D experienced by WK38-3. It is worth noting however that important residual uncertainty is indicated for base parameter b_s (see Table 3).

Unseen verification piles PP-S, PP-W, PP-N

SMC driveability calculations are compared with those determined using the prior parameters for three additional identical production piles at the same location in Figure 18. Similar to the results shown on Figure 13 only the driving energy is varied between these cases, the pile geometry and CPT are identical. The results obtained using the SMC optimised parameters from PP-E are shown to show very good agreement of the penetrations per blow giving confidence in the adopted parameters at this location.

CONCLUSIONS

This study has described an optimisation framework to update uncertain model parameters in axial static design methods for use in the prediction of pile driveability. The proposed approach was demonstrated using a previously published case study from a German offshore wind site. The optimisation process was undertaken using a robust Bayesian approach to dynamically update uncertain variables during driving to improve the match between observed and measured blow count values:.

- Predictions of pile driveability using the prior best estimate of model input parameters provided reasonable estimates of the soil resistance to driving for the higher L/D piles considered in this study giving confidence in the use of axial static design methods to predict SRD. For the lower L/D production piles considered, the prior estimate of model input parameters tended to significantly under-predict the SRD. This highlights the difficulty in transferring existing axial static design approaches to the dynamic pile installation problem directly.

- Bayesian updating was shown to be a very effective option where significant improvements in the mean calculations, and associated variance, of pile driveability was obtained as more data was acquired from each drive. Interestingly, notable differences were observed in the optimised parameter sets for the two pile types indicating additional geoemetrical effects over-and-above those captured in existing static design methods.

- There remain notable discrepancies between the final parameter sets for the different pile geometries. These results suggest additional diameter-dependency or L/D effects in addition to those captured by the methods. Application of the proposed framework to a larger database of pile driving records with a greater range of L/D ratios is warranted to further investigate the trends observed as is consideration

of additional, more advanced, rheological models whose parameters could be included in the vector of uncertain variables given in Eq. 9. Additional considerations related to modelling approach may also be required for larger diameter piles; see Tsetas et al. (2021).

- When compared with predictions determined using a conventional design approach used by industry for static pile capacity, both the prior and optimised parameters achieve notable improvements for both sets of piles. The final updated, optimised parameters can serve as the prior estimates of the model parameters for future drives of similar piles in comparable ground conditions.

This study has shown that, where large-scale pile driving datasets are available the demonstrated optimisation framework has the potential to develop and adapt existing axial capacity methods to account for the salient features observed during pile driving.

Table 1 Hammer parameters adopted in this study

Hammer	m_r (kN)	m_a (kN)	K_c (kN/m)
MHU 800-S	436	146	2.8×10^7
MHU 1200-S	649	304	2.8×10^7

Table 2 Comparison of optimised model parameters with priors: mean values

Parameter	Prior mean	WK38-3		WTG PP-E	
		Mean	Deviation from prior (%)	Mean	Deviation from prior (%)
a_{s1}	0.0125	0.011	-12	0.011	-12
a_{s2}	1.0	0.784	-22	0.958	-4
a_{s3}	0.4	0.355	-11	0.402	0
a_{s4}	0.3	0.262	-4	0.225	-25
b_s	0.15	0.132	-12	0.290	93

Table 3 Comparison of optimised model parameters with priors: COV

Parameter	Prior COV (assumed)	WK38-3		WTG PP-E	
		COV	Deviation from prior (%)	COV	Deviation from prior (%)
a_{s1}	0.3	0.221	-3	0.150	-50
a_{s2}	0.3	0.133	-56	0.266	-11
a_{s3}	0.3	0.162	-46	0.233	-22
a_{s4}	0.3	0.254	-15	0.175	-42
b_s	0.3	0.128	-57	0.307	2

Table 4 Comparison of optimised pile capacities with priors

Pile	Prior		Posterior	
	Shaft (kN)	Base (kN)	Shaft (kN)	Base (kN)
WK38-3	2300	4052	2390	3574
WTG PP-E	3810	9854	4360	19070
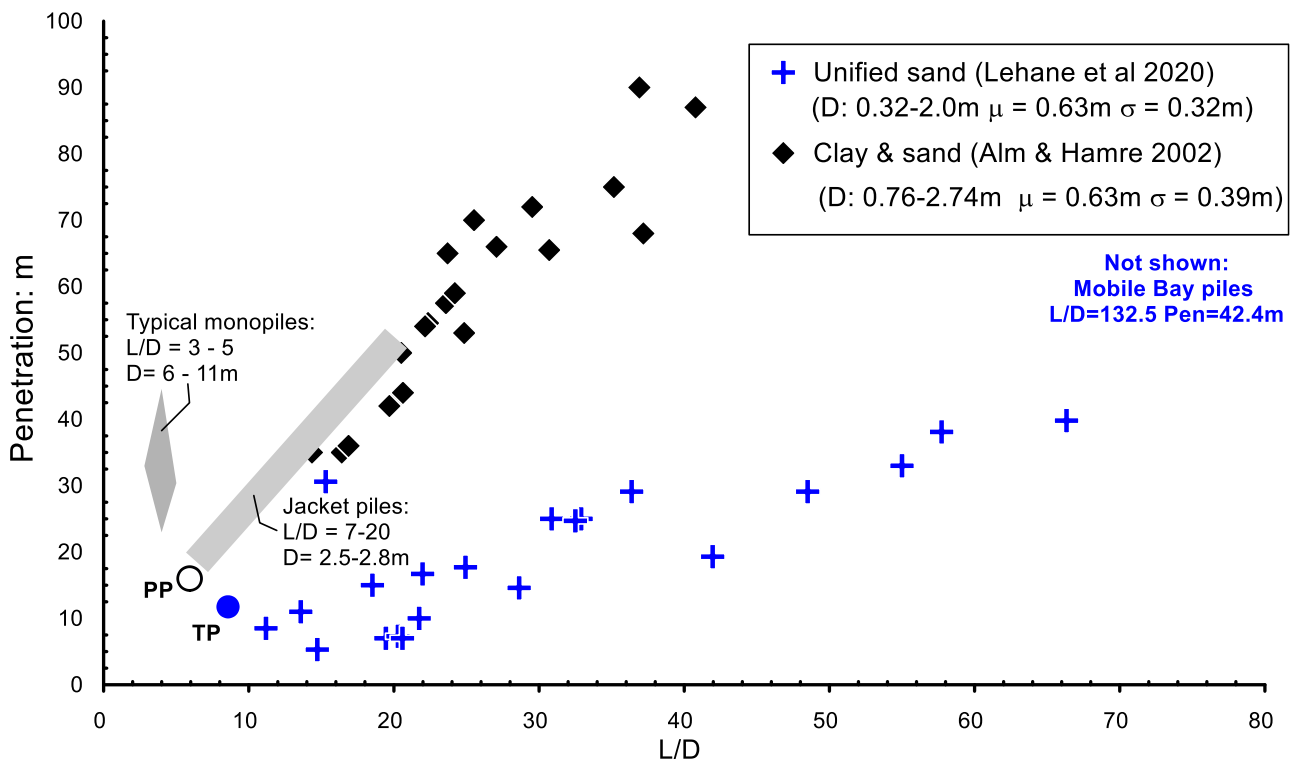
Figure 1 Parameter space of currently available method to predict SRD (Alm and Hamre, 2001) and static axial capacity of open ended tubular piles in sand (Lehane et al., 2020) with typical monopile and jacket pile geometries presently used to support OWT.
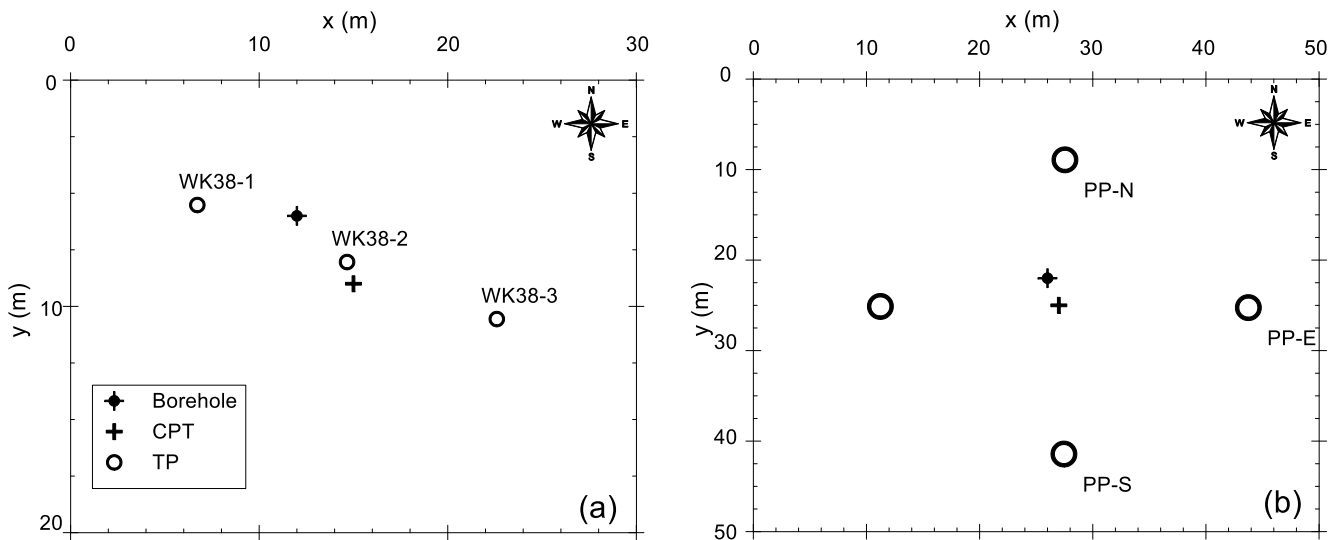
Figure 2 Location of (a) test piles (TP) and (b) production piles (PP) relative to boreholes and CPTs for the cases considered
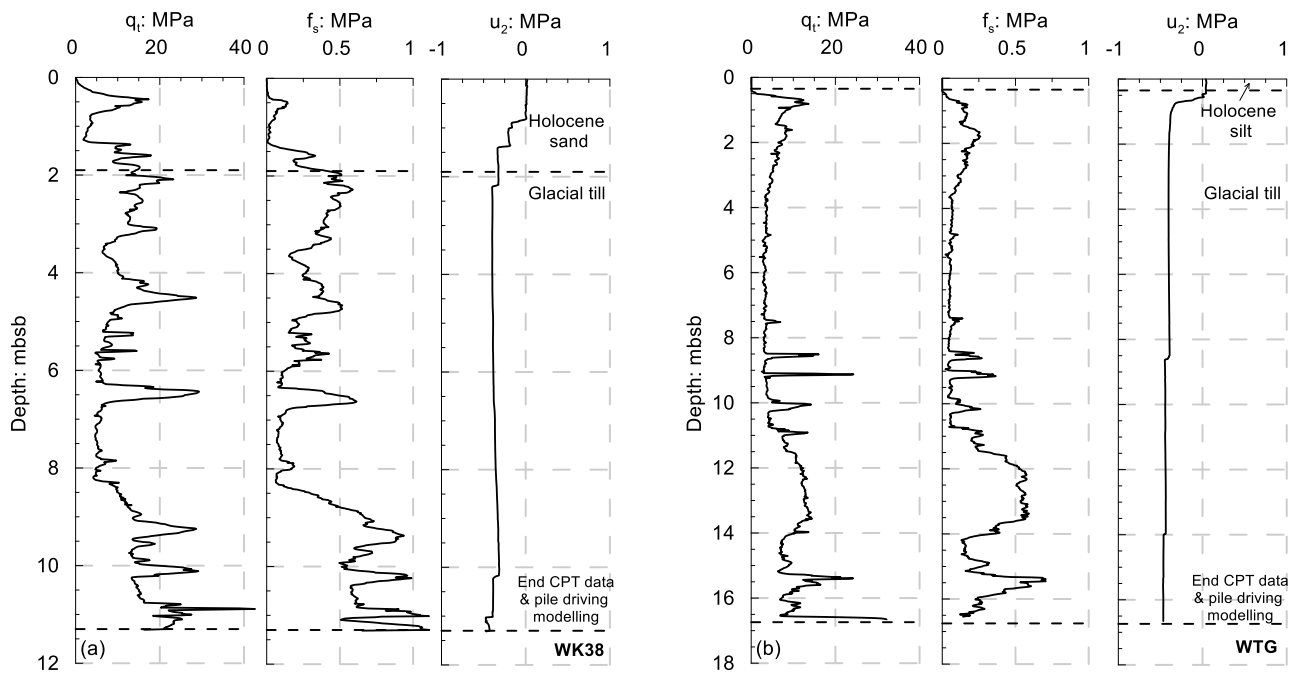
Figure 3 Cone penetration test profiles used in this study for the driveability predictions of piles (a) WK38 (b) WTG-PP
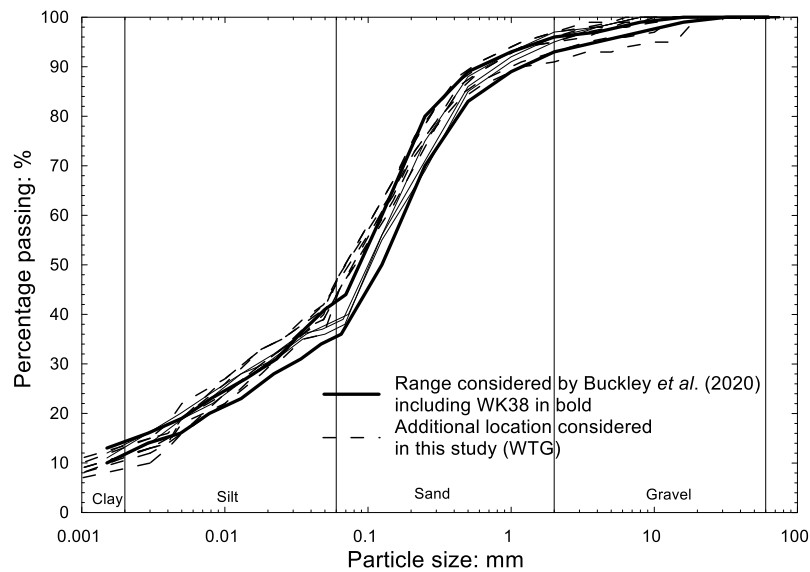
Figure 4 Particle size distributions for locations considered in this study and previous range considered by Buckley et al. (2020)
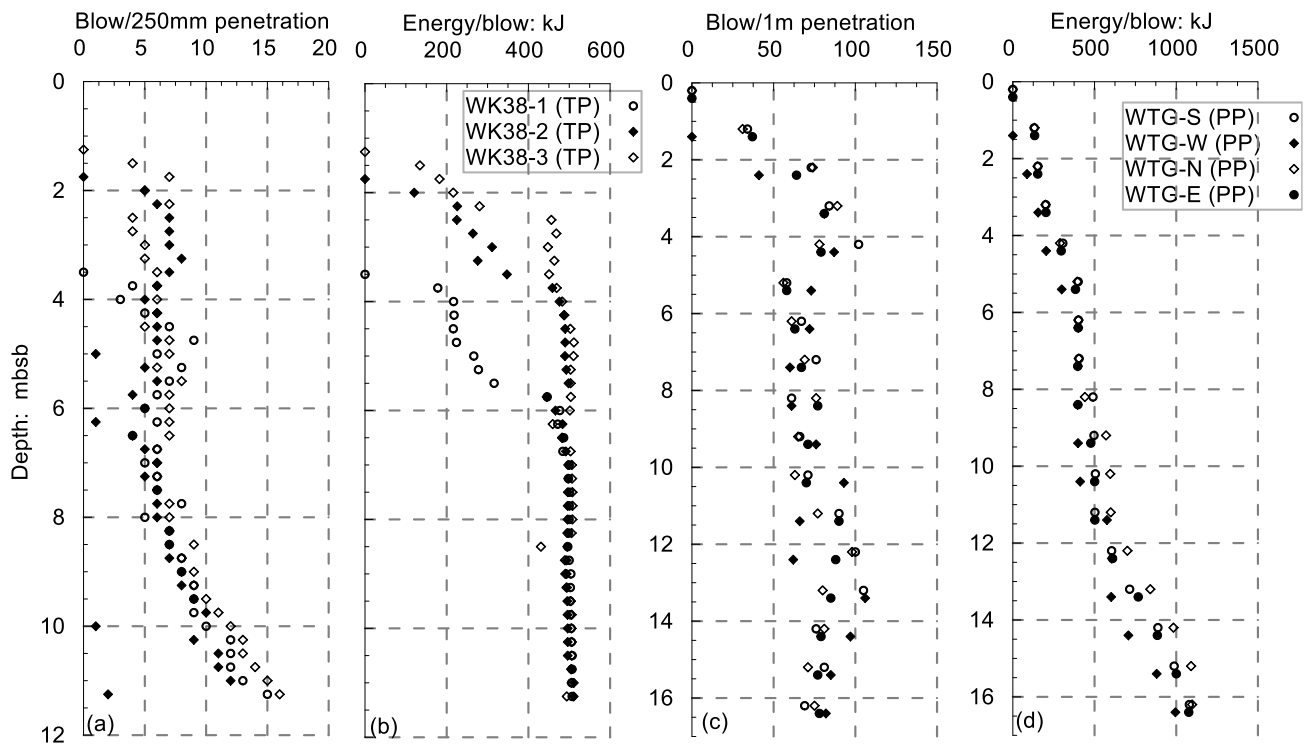
Figure 5 (a) recorded blow counts during TP installation (b) recorded energies during TP installation (c) recorded blow counts during PP installation (d) recorded energies during PP installation
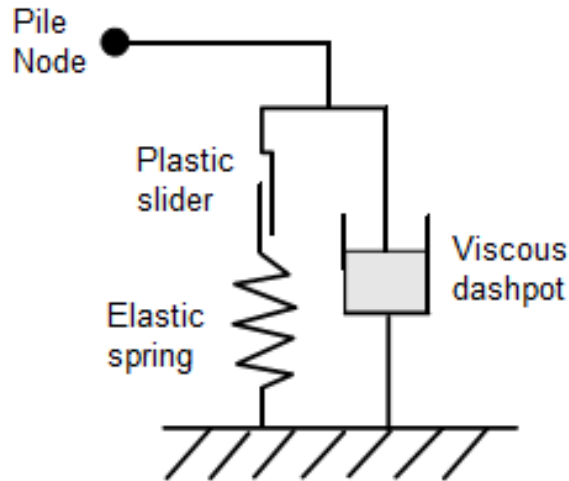
Figure 6 Traditional soil resistance models; adapted from Smith (1962)
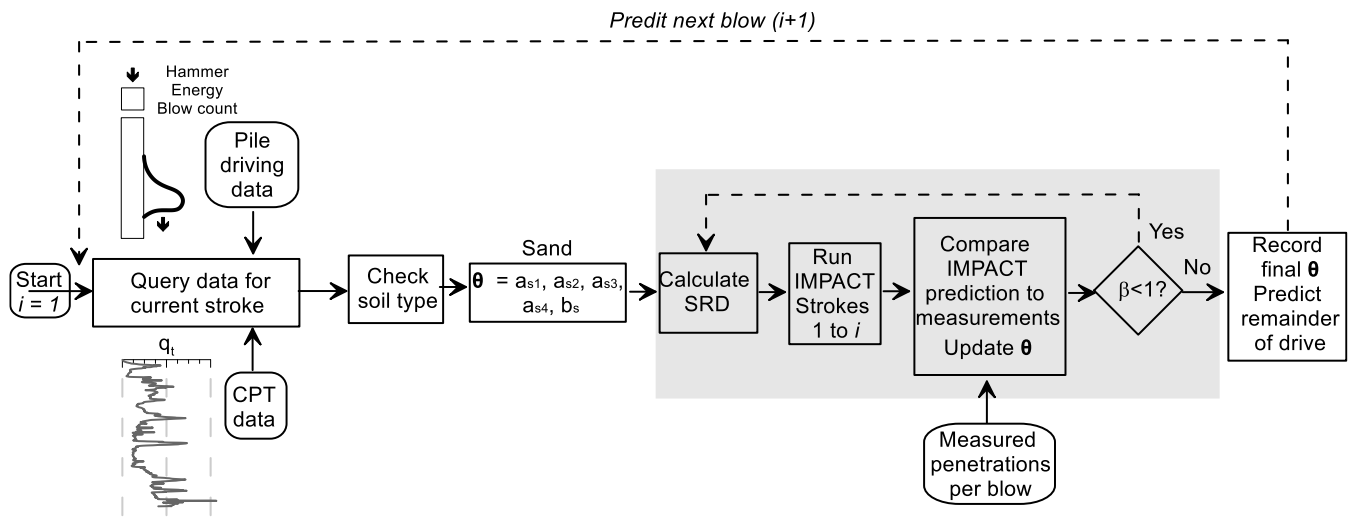
Figure 7 Model parameter updating framework (β is the tempering parameter)
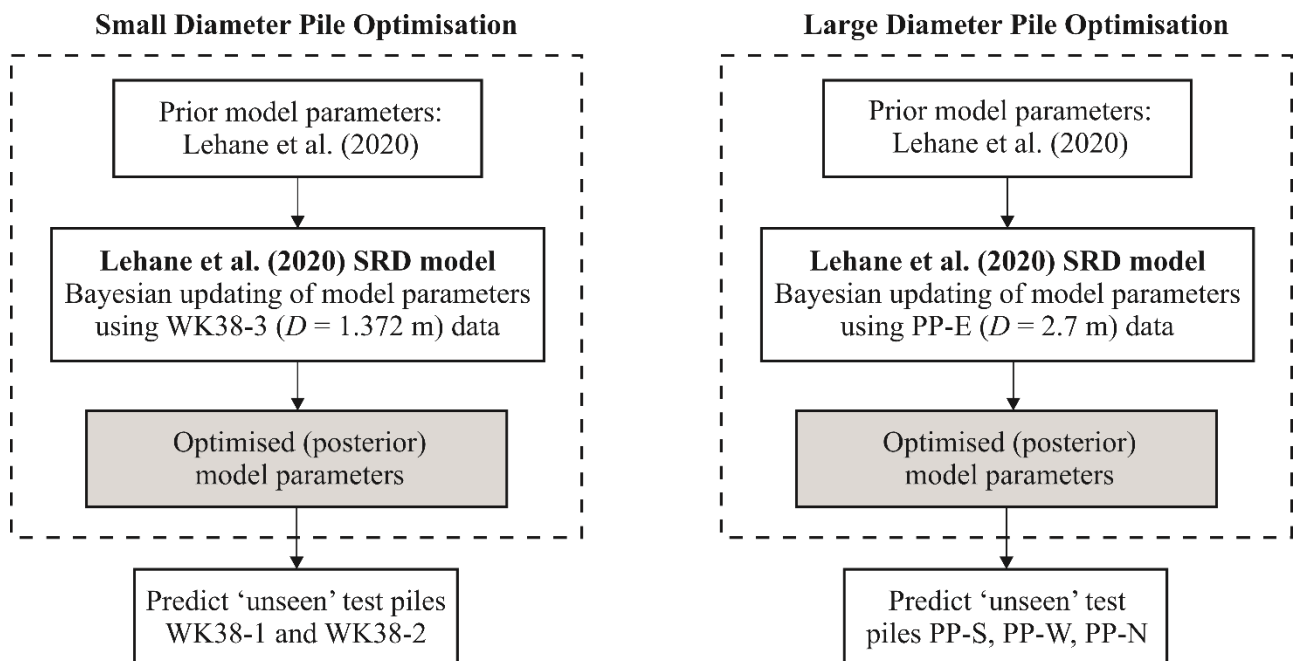
Figure 8 Illustration of adopted framework for optimisation of SRD model parameters based on pile installation data from TP and PP
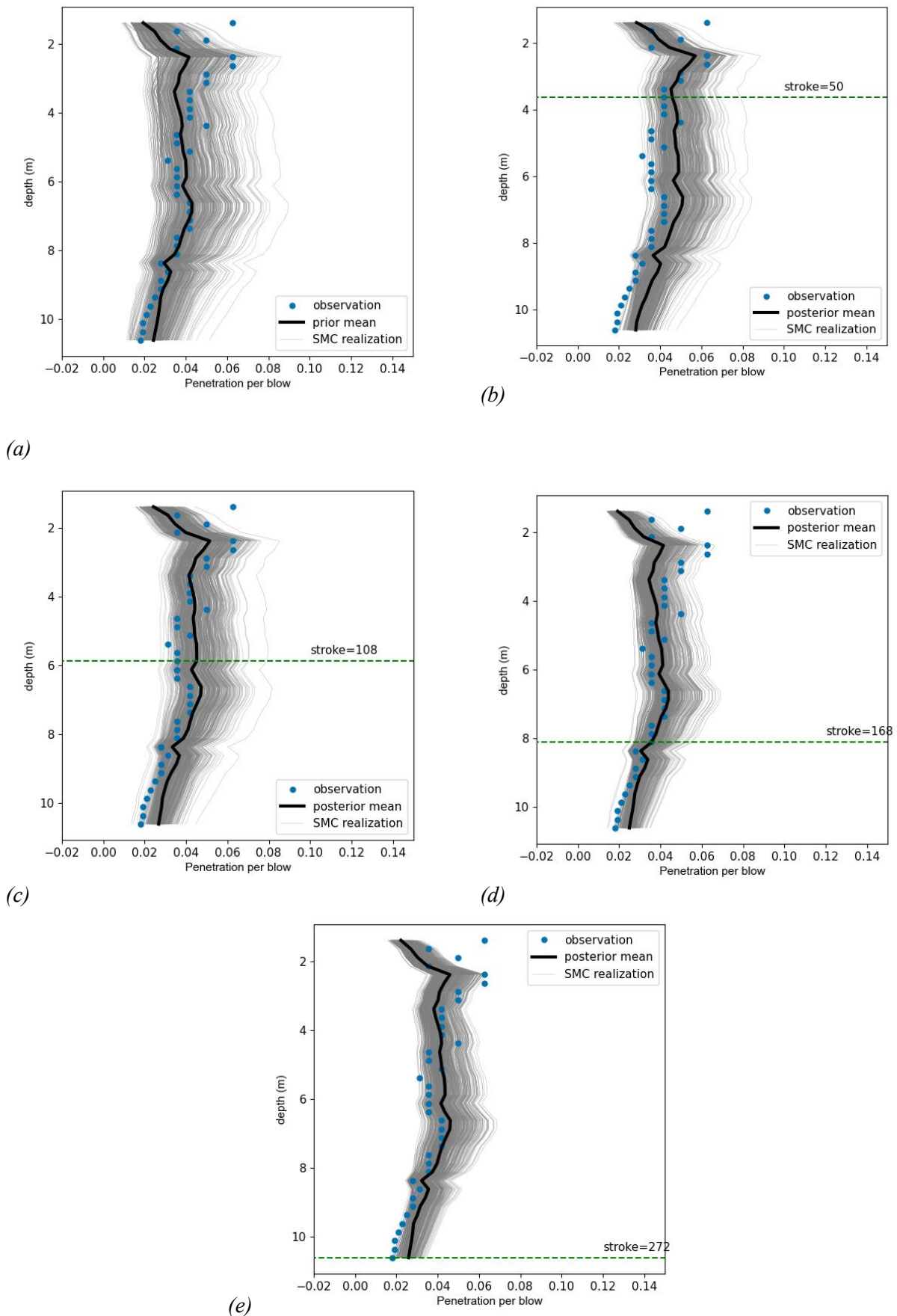
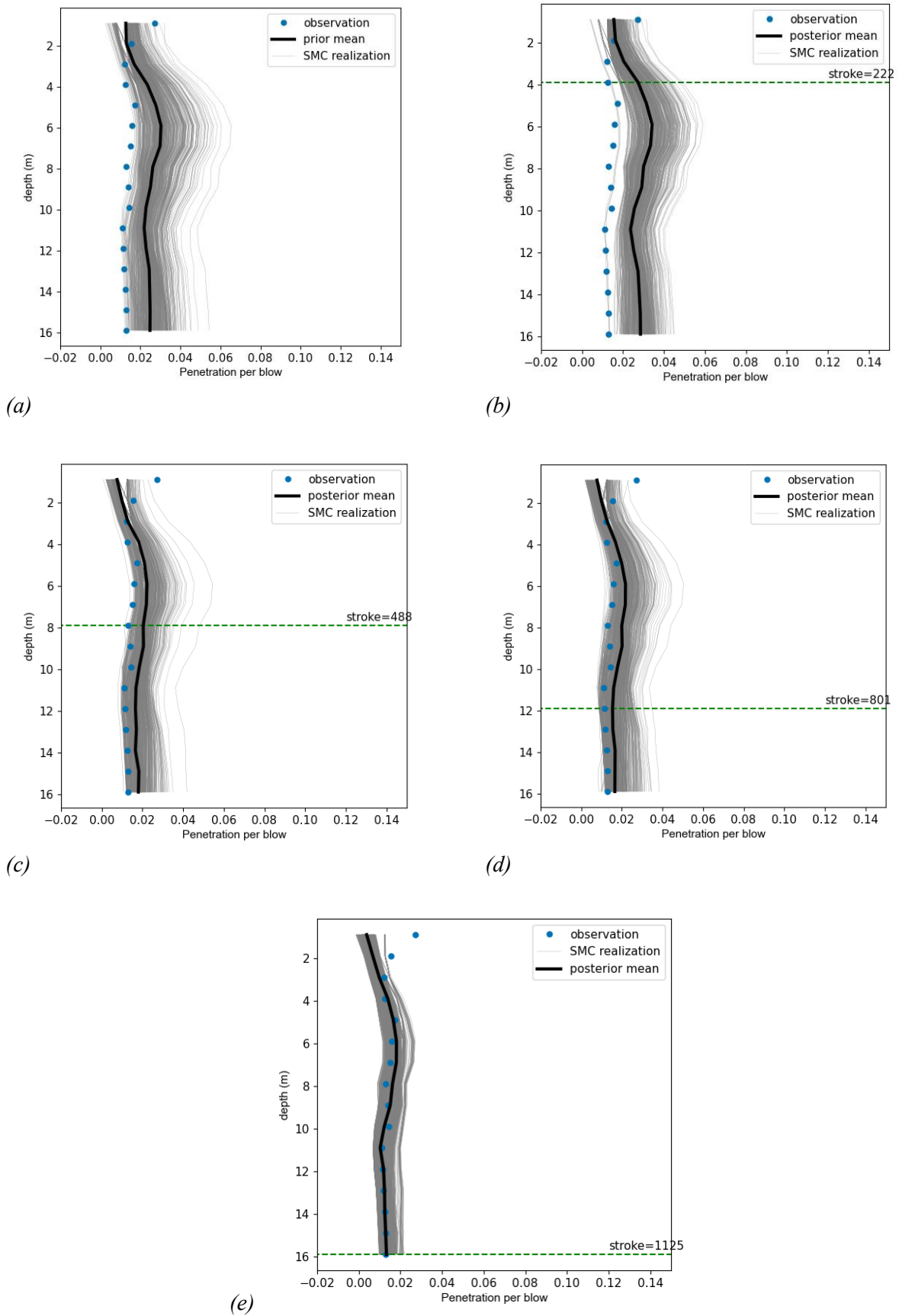*Figure 9 Model predictions of pile driveability using updated model parameters at various points during the installation of WK38-3: (a) prior predictions (at stroke 0), and posterior predictions at strokes equivalent to (b) 25% (c) 50% (d) 75% and (e) 100% of final penetration. SMC model realisations represent predictions determined from 500 draws of the posterior distribution of $\boldsymbol{\theta}$*
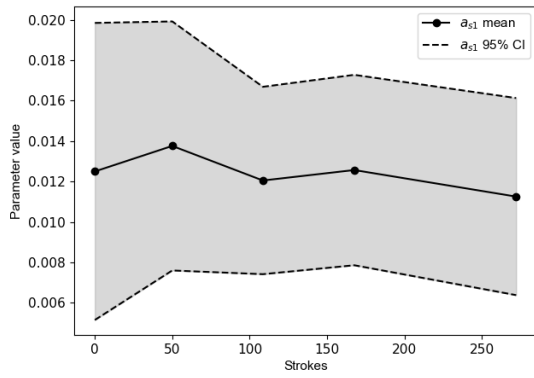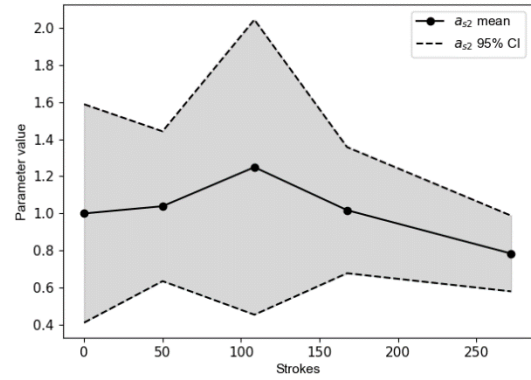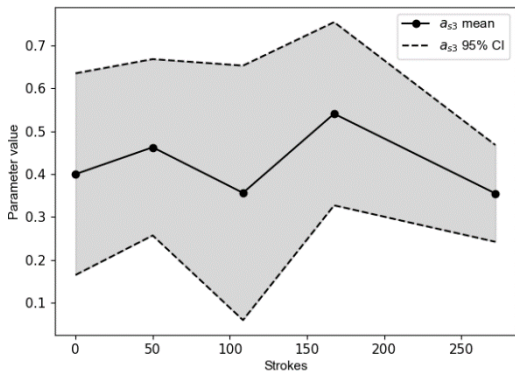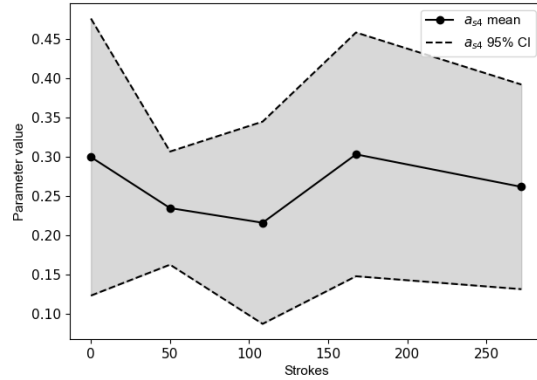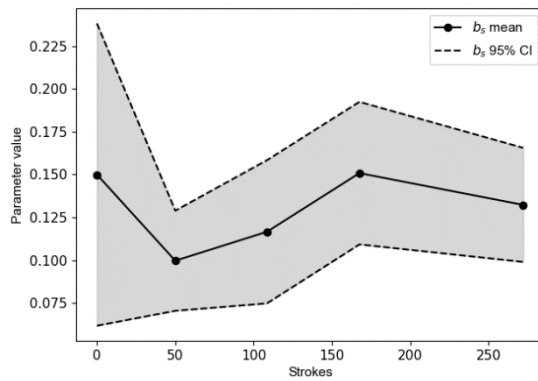
Figure 10 Variation of updated model parameters during the installation of WK38-3 determined using the SMC approach: (a) a_{s1}, (b) a_{s2}, (c) a_{s3}, (d) a_{s4} and (e) b_s.

(a)

(b)

(c)

(d)

(e)
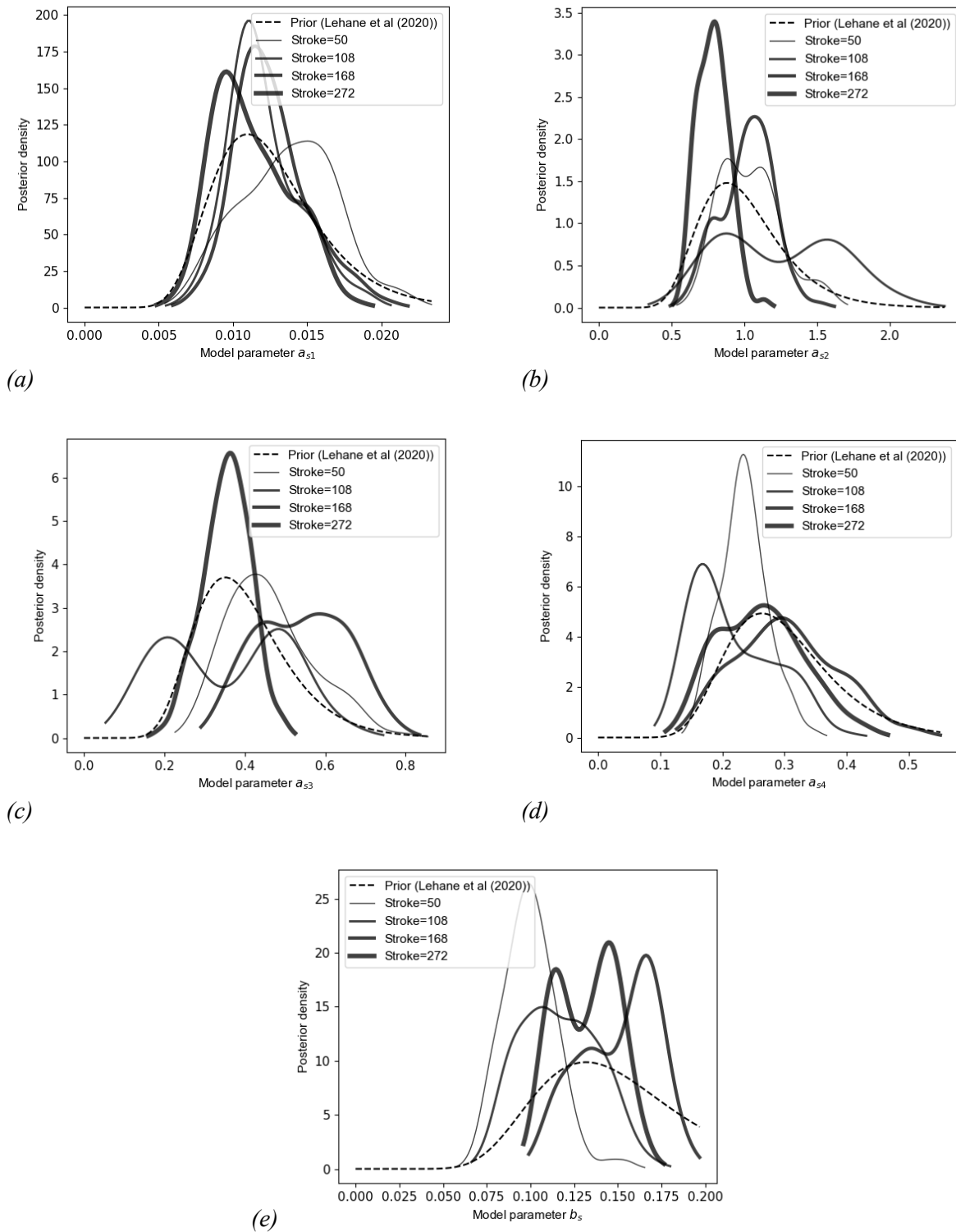
Figure 11 Posterior distributions of model parameters during the installation of WK38-3 determined using the SMC approach: (a) as1, (b) as2, (c) as3, (d) as4 and (e) bs.
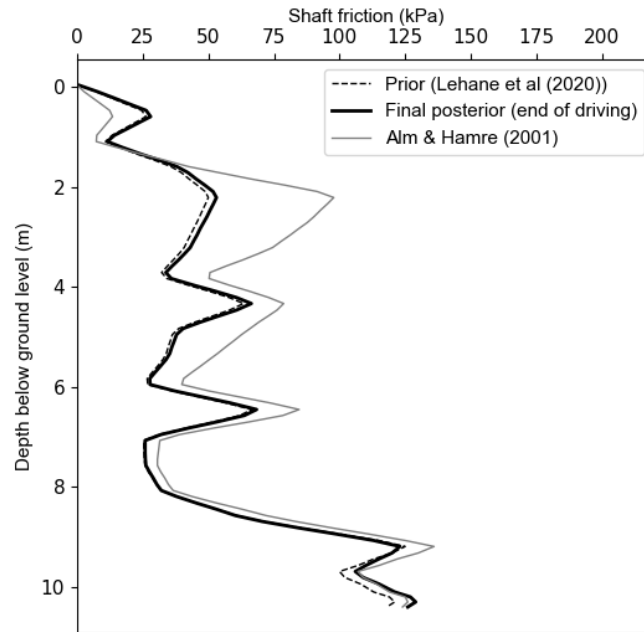
Figure 12 *Model predictions of WK38-3 pile shaft friction at the end of driving using prior and final posterior model parameters compared with predictions determined using industry-standard Alm and Hamre (2001)*
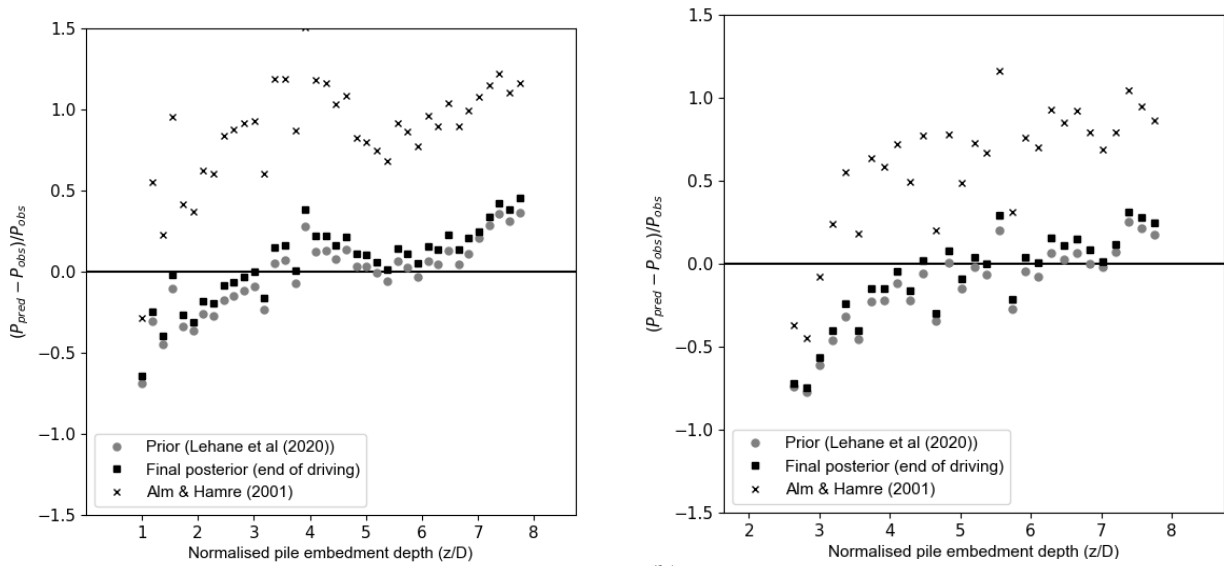
(a)

(b)
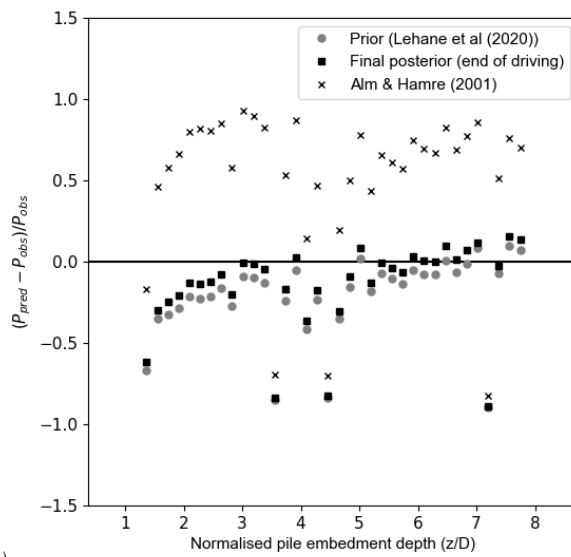
(c)

Figure 13 Comparison of model predictions of pile driveability for (a) WK38-3 (calbration pile) (b) unseen verification pile WK38-1 and (c) unseen verification pile WK38-2

(a)

(b)

(c)

(d)

(e)

Figure 14 Model predictions of pile driveability using updated model parameters at various points during the installation of PP-E- (a) prior predictions (at stroke 0), and posterior predictions at strokes equivalent to (b) 25% (c) 50% (d) 75% and (e) 100% of final penetration. SMC model realisations represent predictions determined from 500 draws of the posterior distribution of θ.
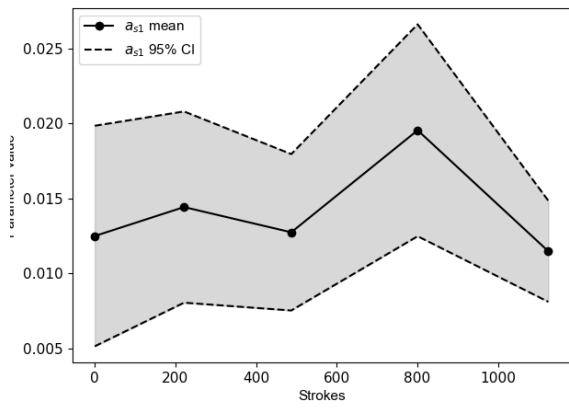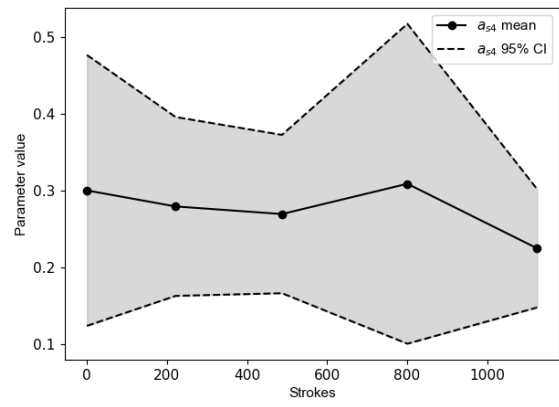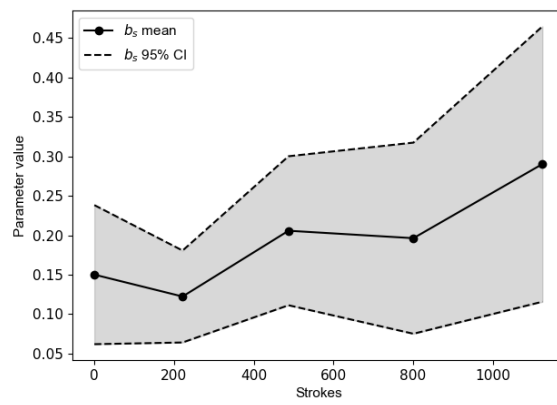
(a)
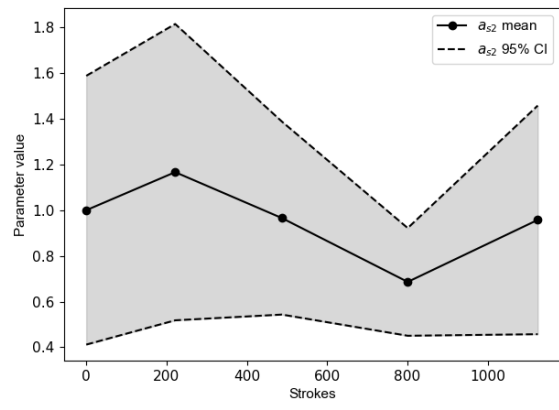
(b)
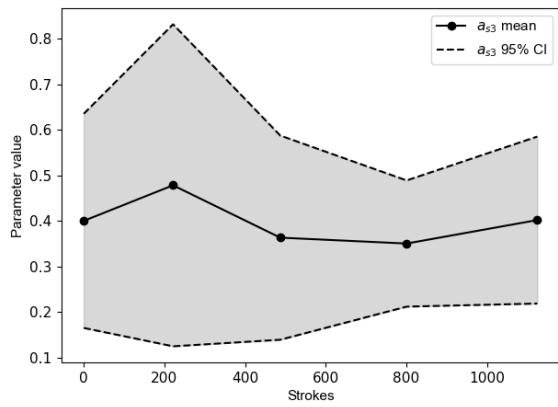
(c)

(d)

(e)

Figure 15 Variation of updated clay model parameters during the installation of PP-E determined using the SMC approach: (a) a_{s1}, (b) a_{s2}, (c) a_{s3}, (d) a_{s4} and (e) b_s.
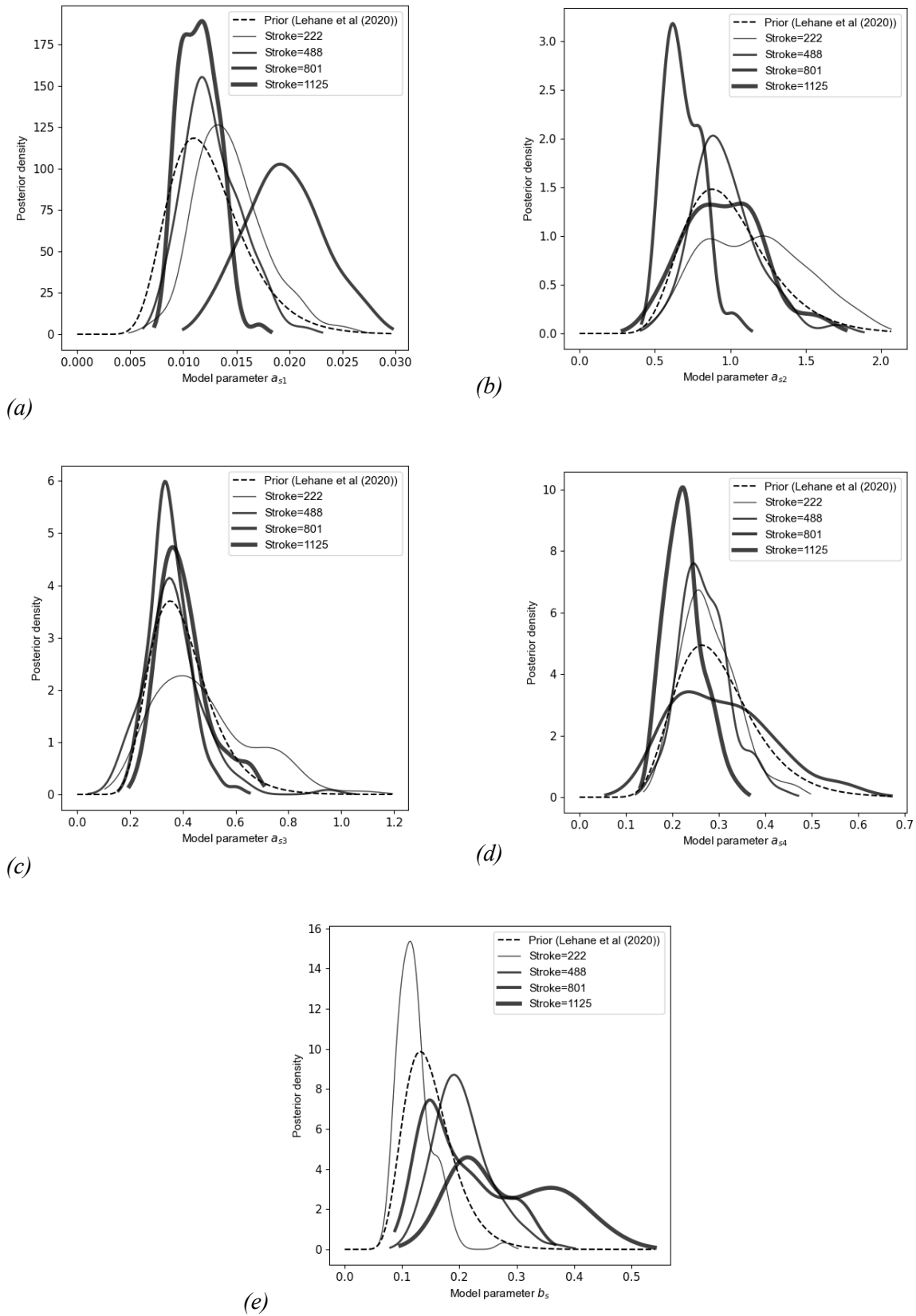
Figure 16 Variation of updated clay model parameters during the installtion of PP-E determined using the SMC approach: (a) a_{s1}, (b) a_{s2}, (c) a_{s3}, (d) a_{s4} and (e) b_s.
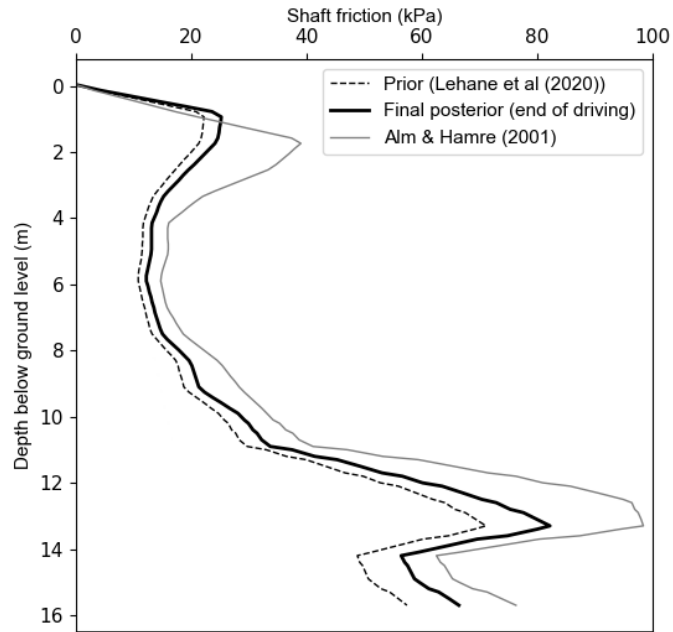
Figure 1*7 Model predictions of WTG-A PP shaft friction at the end of driving using prior and final posterior model parameters compared with predictions determined using industry-standard Alm and Hamre (2001)*
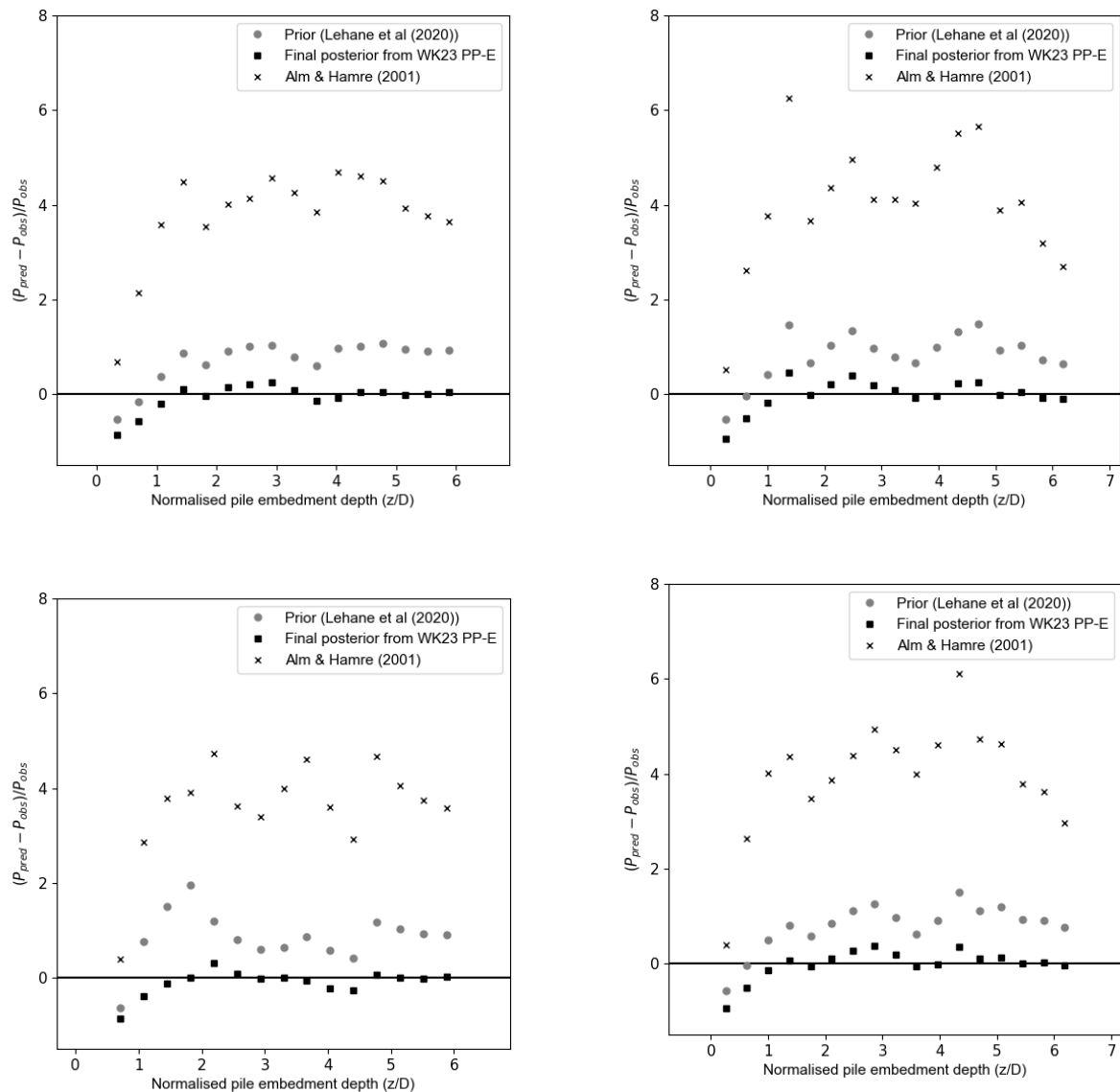
Figure 18 Comparison of model predictions of pile driveability for (a) calibration pile PP-E (b) unseen verification PP-S (c) unseen verification PP-W (d) unseen verification PP-N

REFERENCES

Alm, T. & Hamre, L. Soil model for pile driveability predictions based on CPT interpretations. Proc. 15th Intl. Conf. Soil Mech. Geotech. Eng., 2001 Istanbul, Turkey. Balkema, 1297-1302.

Api 2014. API RP 2A-WSD:Recommended practice for planning, designing and constructing fixed offshore platforms – working stress design, 22nd edition. Washington D,C., USA: American Petroleum Institute.

Barbosa, P. 2021. *RE: Personal Communication.*

Barbosa, P., Geduhn, M., Jardine, R. J., Schroeder, F. C. & Horn, M. Offshore pile load tests in chalk. *In:* WINTER, M. G., ed. Proc. 16th Eur. Conf. Soil Mech. Geotech. Eng., 2015 Edinburgh, Scotland. ICE Publishing, 2885-2890.

Buckley, R. M. 2018. *The axial behaviour of displacement piles in chalk.* PhD, Imperial College London.

Buckley, R. M., Jardine, R. J., Kontoe, S., Barbosa, P. & Schroeder, F. C. 2020. Full-scale observations of dynamic and static axial responses of offshore piles driven in chalk and tills. *Géotechnique,* 70**,** 657-681.

Buckley, R. M., Kontoe, S., Jardine, R. J., Maron, M., Schroeder, F. C. & Barbosa, P. Common pitfalls of pile driving resistance analysis - A case study of the Wikinger offshore windfarm. *In:* POWELL, T., ed. Proc. 8th Intl. Conf. Offshore Site Investigation and Geotechnics, 2017 London, UK. London, UK: Society of Underwater Technology, 1246-1253.

Buckley, R. M., Kontoe, S., Jardine, R. J., Schroeder, F. C. & Barbosa, P. 2021. Pile driveability in low to medium density chalk. *Canadian Geotechnical Journal,* 58**,** 650-665.

Byrne, B. W., Burd, H. J., Gavin, K. G., Houlsby, G. T., Jardine, R. J., Mcadam, R. A., Martin, C. M., Potts, D. M., Taborda, D. M. & Zdravkovic, L. PISA: Recent developments in offshore wind turbine monopile design. Proceedings of the 1st Vietnam Symposium on Advances in Offshore Engineering: Energy and Geotechnics, 2018. Springer, 350-355.

Byrne, T., Doherty, P., Gavin, K. & Overy, R. Comparison of Pile Driveability Methods In North Sea Sand. *In:* POWELL, T., ed. Proc. 7th Intl Conf. Offshore Site Invesigations and Geotechnics, 2012 London, UK. Society of Underwater Technology, 481-488.

Ching, J. & Chen, Y.-C. 2007. Transitional Markov chain Monte Carlo method for Bayesian model updating, model class selection, and model averaging. *Journal of engineering mechanics***,** 816-832.

Collico, S., Arroyo, M., Kopf, A. & Devincenzi, M. 2022. A probabilistic Bayesian methodology for the strain-rate correction of dynamic CPTu data. *Canadian Geotechnical Journal*.

De Josselin De Jong, G. 1956. Wat gebeurt er in de grond tijdens het heien. *De Ingenieur,* 68**,** B77-B88.

Deeks, A. & Randolph, M. 1993. Analytical modelling of hammer impact for pile driving. *International Journal for Numerical and Analytical Methods in Geomechanics,* 17**,** 279-302.

Gavin, K. & Lehane, B. M. 2007. Base load-displacement response of piles in sand. *Can. Geotech. J.,* 44**,** 1053-1063.

Heerema, E. P. Predicting pile driveability: heather as an illustration of the friction fatigue theory. Proc. Eur. Offshore Petroleum Conf., 1978 London, UK. Society of Petroleum Engineers, 413-422.

Hsein Juang, C., Luo, Z., Atamturktur, S. & Huang, H. 2013. Bayesian updating of soil parameters for braced excavations using field observations. *Journal of Geotechnical and Geoenvironmental Engineering,* 139**,** 395-406.

Hsiao, E. C., Schuster, M., Juang, C. H. & Kung, G. T. 2008. Reliability analysis and updating of excavation-induced ground settlement for building serviceability assessment. *Journal of Geotechnical and Geoenvironmental Engineering,* 134**,** 1448-1458.

Jardine, R. J., Buckley, R. M., Liu, T. F., Byrne, B. W., Kontoe, S., J.;, Mcadam, R. A., Schranz, F. & Vinck, K. 2023. The axial behaviour of piles driven in chalk - Géotechnique - in press.

Jardine, R. J., Chow, F. C., Overy, R. & Standing, J. R. 2005. *ICP design methods for driven piles in sands and clays,* London, Thomas Telford.

Jaynes, E. T. & Bretthorst, G. L. 2003. *Probability theory: The logic of science*, Cambridge university press.

Kaynia, A. M., Hebig, J., Pein, T. & Shin, Y. 2022. Numerical model for dynamic installation of large diameter monopiles. *Soil Dynamics and Earthquake Engineering,* 161**,** 107393.

Lehane, B., Liu, Z., Bittar, E., Nadim, F., Lacasse, S., Jardine, R., Carotenuto, P., Jeanjean, P., Rattley, M. & Gavin, K. A new 'unified' CPT-based axial pile capacity design method for driven piles in sand. *In:* WESTGATE, Z. J., ed. 4th International Symposium on Frontiers in Offshore Geotechnics, 2020 Austin, Texas. American Society of Civil Engineers, 463-477.

Li, X., Zhang, L., Jiang, S., Li, D. & Zhou, C. 2016. Assessment of slope stability in the monitoring parameter space. *Journal of Geotechnical and Geoenvironmental Engineering,* 142**,** 04016029.

Lumb, P. 1966. The variability of natural soils. *Canadian Geotechnical Journal,* 3**,** 74-97.

Maynard, A., Hamre, L., Butterworth, D. & Davison, F. Improved Pile Installation Predictions for Monopiles. *In:* BULLOCK, P. V., G.; TARA, D.; PAIKOWSKY,S., ed. 10th International Conference on Stress Wave Theory and Testing Methods for Deep Foundations, 2018 San Diego, California. ASTM International, 426-449.

Minson, S., Simons, M. & Beck, J. 2013. Bayesian inversion for finite fault earthquake source models I— Theory and algorithm. *Geophysical Journal International,* 194**,** 1701-1726.

Perikleous, G., ;, Stergiou, T. & Meissl, S. An assessment of the accuracy of SRD methodologies for OWF monopile installation against a North Europe driving records database. *In:* WESTGATE, Z. J., ed. 4th Intl Symposium on Frontiers in Offshore Geotechnics, 2020 Austin, Texas. Deep Foundations Institute, 704-713.

Qi, X.-H. & Zhou, W.-H. 2017. An efficient probabilistic back-analysis method for braced excavations using wall deflection data at multiple points. *Computers and Geotechnics,* 85**,** 186-198.

Randolph, M. F. 1990. Analysis of the dynamics of pile driving. *Developments in Soil Mechanics IV: Advanced Geotechnical Analyses.* Elsevier.

Randolph, M. F. 2008. IMPACT - Dynamic analysis of pile driving.

Salgado, R., Loukidis, D., Abou-Jaoude, G. & Zhang, Y. 2015. The role of soil stiffness non-linearity in 1D pile driving simulations. *Géotechnique,* 65**,** 169-187.

Schneider, J. A. & Harmon, I. A. 2010. Analyzing Drivability of Open Ended Piles in Very Dense Sands. *DFI Journal,* 4**,** 32-44.

Siegl, K., Dührkop, J. & Spill, S. 2020. A design framework for monopiles in sand based on large-scale pile load tests and FE analysis. *In:* WESTGATE, Z. J. (ed.) *4th Intl Symposium on Frontiers in Offshore Geotechnics.* Austin, Texas: Deep Foundations Institute

Simons, H. A. & Randolph, M. F. 1985. A new approach to one dimensional pile driving analysis. *Intl. Conf. on Numerical Methods in Geomechanics.* Nagoya, Japan.

Smith, E. a. L. 1962. Pile-driving analysis by the wave equation. *J. Soil Mech Found. Eng. - ASCE,* 4**,** 35-61.

Stevens, R. S., Wiltsie, E. A. & Turton, T. H. Evaluating drivability for hard clay very dense sand and rock. Offshore Technology Conference, 1982 Houston, Texas. Offshore Technology Conference, 465-483.

Toolan, F. E. & Fox, D. A. 1977. Geotechnical plannig of piled foundations for offshore platforms. *Proc of the ICE - Civil Engineering,* 62**,** 221-244.

Tsetas, A., Tsouvalas, A. & Metrikine, A. V. 2021. Installation of large-diameter monopiles: Introducing wave dispersion and non-local soil reaction. *Journal of Marine Science and Engineering,* 9**,** 313.

Zhang, L., Tang, W. & Zhang, L. 2009. Bayesian model calibration using geotechnical centrifuge tests. *Journal of geotechnical and geoenvironmental engineering,* 135**,** 291-299.

Zheng, D., Huang, J., Li, D.-Q., Kelly, R. & Sloan, S. W. 2018. Embankment prediction using testing data and monitored behaviour: A Bayesian updating approach. *Computers and Geotechnics,* 93**,** 150-162.